Progress in Photovoltaics: Research and Applications

WILEY

PROGRESS IN PHOTOVOLTAICS

RESEARCH ARTICLE

Electrical Performance, Loss Analysis, and Efficiency Potential of Industrial-Type PERC, TOPCon, and SHJ Solar Cells: A Comparative Study

Qinqin Wang[1] | Kaiyuan Guo[1] | SiWen Gu[2] | Wei Huang[1] | Hui Peng[1] | Wangping Wu[2] | Jianning Ding[1]

[1]Institute of Technology for Carbon Neutralization, Yangzhou University, Yangzhou, China | [2]Jiangsu Collaborative Innovation Center of Photovoltaic Science and Engineering, Changzhou University, Changzhou, China

Correspondence: Qinqin Wang (wangqinqin@yzu.edu.cn) | Jianning Ding (dingjn@yzu.edu.cn)

Received: 10 February 2024 | **Revised:** 7 July 2024 | **Accepted:** 17 July 2024

Funding: This work has been partially supported by the National Key Research and Development Program of China (2023YFB4202600, 2023YFB4202605) and the National Natural Science Foundation Youth Project (62304199).

Keywords: heterojunction back-contact | loss analysis | passivating selective contacts | theoretical limiting efficiency | TOPCon back-contact

ABSTRACT

Currently, the efficiency of p-type passivated emitter and rear contact (PERC) cells has been growing at an absolute efficiency of 0.5% per year and has reached 23%–23.5% in mass production while getting closer to its theoretical efficiency limit. n-Type tunnel oxide passivated contact (TOPCon) and silicon heterojunction (SHJ) cells with their superior "passivating selective contacts" technology were the most interesting photovoltaics (PV) technology in the industry. The effect of different passivated contact layers with respect to their influence on the J_0, $J_{0,metal}$, ρ_c, and the carrier selectivity (S_{10}) and the loss analysis and efficiency potential of industrial-type PERC, TOPCon, and SHJ solar cells were studied and compared. The results showed that TOPCon structure with a high passivation performance and good optical performance is more suitable for bifacial solar cell and the highest theoretical limiting efficiency with metal shading on the n-type Si wafer ($\eta_{b,e,h,m,max}$) can be achieved to 27.62%. Although SHJ structure with the highest passivation performance but the worst optical performance owing to the parasitic absorption of a-Si:H layer and high contact resistivity, the value of $\eta_{b,e,h,m,max}$ is 0.7% lower than that of TOPCon solar cells. PERC structure has superior optical performance than SHJ structure, but due to poor passivation performance, the $\eta_{b,e,h,m,max}$ is only 26.42%. The next-generation products may be heterojunction back-contact (HBC) and TOPCon back-contact (TBC) cells with high $\eta_{b,e,h,m,max}$ of 28.12% and 27.99%, respectively. Exploiting a perfect passivation of the noncontact area, the wide process window and low cost are required and transferring these new concepts to industrial solar cell production will be the next major challenge.

1 | Introduction

The solar industry has been attracting attention as a future energy source. Crystalline silicon (c-Si) has the unique features, such as nontoxicity, abundant source, and long-term stability, which has made it a market-dominant technology with an almost 95% market share [1]. The passivated emitter and rear contact (PERC) cells are derived from the conventional aluminum back surface field (Al-BSF) structure, which was developed by Green et al. at the University of New South Wales (UNSW) in 1989 [2]. However, this technology took 30 years to achieve large-scale production. The production capacity of PERC cells has grown exponentially, and the market share of PERC p-type mono-Si was 80% in 2022 according to the International Technology Roadmap for Photovoltaics (ITRPV) [3]. The efficiency of p-type monocrystalline PERC cells has been increasing at an absolute efficiency of 0.5% per year [4] and has reached 23%–23.5% in large-scale production [5, 6]. The rapid increase in cell efficiency cannot be attributed to improvements

[Correction added on 19 September 2024, after first online publication: The second corresponding author has been changed from 'Wangping Wu' to 'Jianning Ding' in this version.]

in device structure alone; at the same time, it is a combination of some aspects of the cell manufacturing process. Starting from the substrate material, thinner and higher quality Si wafers with lower impurity concentrations and crystal defects greatly suppress the loss of substrate composite materials and provide a prerequisite for manufacturing high-efficiency solar cells. The development and implementation of processes to mitigate boron–oxygen (B–O)-related light-induced degradation (LID) as well as photothermal attenuation (LeTID) [7–9] in Ga-doped p-type direct-drawn silicon (Cz) growth [10, 11] have improved the long-term stability of PERC solar cells. In addition, improvements in surface passivation materials and techniques, such as the use of thermally grown silicon dioxide (SiO_2)/silicon nitride (SiN_x:H) stacked layers on the front surface [12–15] and AlO_x/SiN_x layers on the back surface [16–18], have reduced carrier recombination on the surface. The introduction of selective emitter (SE) structures can effectively separate the requirement to form high-quality ohmic contacts from the design of diffuse emitters in the passivation region [19–22]. These regions function as membranes that block minority carriers and conduct majority carriers [23] and thereby define the direction of current flow and make the solar cell work. Heavy doping (n^{++}) forms a local electric field on the surface silicon, sweeping holes back into the c-Si and accelerating electron conduction to the electrode [24]. Subsequently, more lightly doped emitters and screen-printed silver pastes designed to form effective contacts with such emitters have been used in PERC cells, resulting in improved front surface passivation and spectral response without compromising contact resistance. In addition, the developments in screen printing techniques, such as knotless screen printing, dual printing, twice printing, multibusbar technology, and reduced finger widths, have been developed to reduce the optical and resistive losses in the front grid lines [25–28], which can significantly improve the efficiency of PERC cells.

In 2019, LONGi reported efficiencies of 23.83% and 24.06% [29] for champion PERC cells. In 2022, Trina announced that the high-efficiency PERC solar cell with size of 210×210 mm has an efficiency of 24.5%, which is also the highest efficiency record of the PERC structure so far [30]. This efficiency reached 24.5% of the PERC theoretical performance efficiency calculated by Schmidt et al. [31], and the PERC structure had reached the technical bottleneck. The passivated emitter with rear locally diffused (PERL) solar cell, as an upgraded structure of the PERC solar cell, diffuses over the back metallized contact area to form a local p^+ structure. In 2009, the UNSW published PERL's highest efficiency record of 25.0% [32]. However, the average efficiency of the industry's mass-produced PERC solar cells is much lower than the champion efficiency. Most of the losses are recombination at the metal contacts and the loss caused by two- or three-dimensional current transport paths. Therefore, passivation contact has been a hot research topic in the photovoltaics (PV) industry. Currently, the TOPCon structure consists of an ultrathin silicon oxide (SiO_x) film and a $n^{(+)}$-doped polysilicon (poly-Si) layer, which utilizes the concept of tunnel selective engineering. Martin Green first proposed the concept of "passive contact." In 1972, Green et al. [33] showed how tunneling a metal oxide semiconductor (MOS) contact could increase the open-circuit voltage (V_{oc}) by more than 60 mV over a standard p–n junction. In 1981, Martin Green and his group are the first to propose the passivation contact structure with doped poly-Si/SiO_x/Si, and in 1983, they disclosed an 18% efficiency based on this structure, which was the first polycrystalline silicon–based solar cell [34]. However, in the following decades, the study of "passivation contact" has not been widely concerned and applied. Regarding the notation, "poly-Si emitters" or "semi-insulating poly-Si (SIPOS) emitters" [35, 36] were used in the first reports of this contact scheme. What triggered the public rediscovery of "TOPCon" was Feldman and Fraunhofer, who reported in 2013 that TOPCon had replaced BSF, with V_{OC} elevated to 698 mV [37]. Since then, polysilicon/silicon oxide contacts have been reintroduced into the field of solar cells. TOPCon structure is achieved by introducing tunneling barriers (such as ultrathin dielectric layers) into selective contact structures, resulting in asymmetric tunneling probabilities of electrons and holes (such as due to changes in barrier height or effective tunneling mass). For example, it has been proven that ultrathin SiO_2 layers have a larger hole tunneling barrier compared to electrons [38]. TOPCon solar cells have become one of the prospective technologies in the PV market [39]. At present, TOPCon solar cell is one of the mainstream products with a median efficiency of 25%–26% [40]. This is due to advancements in surface passivation materials, structures, and technology, including the use of AlO_x/SiN_x layers on the front surface, boron SE structures with high concentration doping beneath in the metal contact area and low concentration doping in the uncontacted area [41, 42], multi-busbar technology [43], laser-enhanced contact optimization (LECO) technology, a low-corrosion paste to reduce passivation layer damage [44], laser irradiation generated carriers and formed current with a reverse voltage, contact area optimization [45–47], poly-SE with reducing parasitic absorption while retaining good contact [48, 49], and so on. Meanwhile, SunPower, TetraSun, and Silevo companies were also manufacturing on passivating contact solar cells, with technical information withheld from the public domain. According to the ITRPV [3], the share of p-type mono-Si PERC will decrease to about 10% in the next 10 years. TOPCon will gain market share from about 10% by 2022 up to 60% in the next decade. Based on these results, it took about 10 years to commercialize it. TOPCon on n-type is expected to become the dominating cell concept after 2025. The highest efficiency for n-TOPCon has achieved 26.89% with a specific surface area of 330.15 cm^2 at JinkoSolar [50]. POLO-IBC cells with an efficiency of 26.1% were reported with a specific surface area of 4 cm^2 [51]. There are two key factors limiting the efficiency of TOPCon cells. One is the loss caused by boron heavy doping, which enhances the saturation current density J_0 in the passivated contact region [52], and the other is recombination at the p^+ layer metal contacts, which are a current challenge for PV manufacturing.

SHJ cell technology, the second important n-type passivation contact, which is a structure with a monocrystalline silicon wafer sandwiched between nanometer-thick n-type (p-type) doped hydrogenated amorphous silicon (a-Si:H) layers and passivation and base contacts deposited by low-temperature plasma-enhanced chemical vapor deposition (PECVD) on Si bulk materials, was reported by Walther et al. at the University of Marburg in 1974 [53]. This type of carrier-selective contact is also known as 'heterojunction with intrinsic thin layer' (HIT) contact [54]. The p-type or n-type doping of a-Si:H causes band bending of the work function (WF), leading to carrier selectivity. By selecting functional materials that match the band structure, a high potential barrier for holes and a small or even zero potential barrier for electrons can be directly formed at the

interface, ensuring both J_0 and ρ_c to form the optimal electron selective transport [24]. The first solar cell using a silicon heterojunction was reported in 1983 by Hamakawa et al. in the form of an a-Si:H/poly-Si heterojunction bottom cell in a tandem junction solar cell, called honeymoon cell [55]. At the same time, the electronic junction between doped a-Si:H and c-Si was largely investigated [56]. In the late 1980s, Sanyo (Japan) started to incorporate heterojunctions into c-Si wafer-based solar cells. In recent years, SHJ technology has gained increasing attention within the PV industry due to their high efficiency, low-temperature processes, good temperature coefficients, and high bifacial rates [57–60]. In 2022, LONGi raised the world record power conversion efficiency (PCE) to 26.81% (274cm^2, M6 size) [61], approaching the fundamental limit of single-junction Si solar cells (29.4%) [62]. In 2023, interdigitated back-contact (IBC) structure was combined with the SHJ solar cells, reaching a record PCE of 27.09% [63]. In 2024, LONGi has set a new record for PCE for silicon heterojunction back-contact (HBC) cells, 27.3% [64]. In recent years, with the development of technologies such as nanocrystalline silicon oxide (nc-SiO_x:H) films [65–67], multi-busbar [43], phosphorus (P) gettering [68], and wavelength conversion film [69], more industry participants joined the market of SHJ solar cell. As predicted by the ITRPV [3], SHJ solar cells are expected to gain a 2023 market share of about 9% to over 25% in the next decade. Based on these results, it took about 30 years to commercialize it. At present, some enterprises have carried out mass production of SHJ solar cells, and the mass production efficiency is about 25.0%–25.8% [40]. A trade-off of the cost and output power of SHJ solar cells is still an obstacle to its expanding market share. Being different from any previous scalable c-Si PV generations, the SHJ cell features uniquely indispensable transparent conducting oxide layers integrating a low-temperature annealing metal paste and high equipment investment. The unique electrode and equipment requirement is still the dominant factor to determine its rate of exposure mass manufacture technology [44].

According to ITRPV's prediction [3], it appears that developing the "passivating selective contact" technology has become a hot topic for the next mass production of solar cells. Therefore, the objective of this study was focused on the effect of different passivated contact layers with respect to their influence on the J_0, $J_{0,metal}$, ρ_c, and the carrier selectivity (S_{10}). At the same time, we simulated three types of solar cell (PERC, TOPCon and SHJ), which consisted of screen-printed metallic contacts on both sides fabricated from 182 m×182×0.14 mm Cz-Si wafers through an industrial-type process; further investigated their passivation performance, optical performance, and the *I–V* parameters of solar cells, that is, efficiency (E_{ff}), open-circuit voltage (V_{oc}), fill factor (*FF*), and short-circuit current density (J_{sc}); and finally discussed its current status and future trends.

2 | Experimental

2.1 | Solar Cell Fabrication

We fabricated three types of samples. Figure 1 shows the schematic depiction of the sample structure in order to extract the passivation layer (J_0): (I) the P-doped n^+ sample with a symmetric double-sided P-diffused with SiO_x/SiN_x on 5 Ω·cm p-type Cz-Si wafers; (II) the P-doped n^{++} sample with a symmetric double-sided laser doping the P-doped n^+ sample with SiO_x/SiN_x on 5 Ω·cm p-type Cz-Si wafers; (III) the B-doped p^+ sample with a symmetric double-sided B-diffused and passivation with AlO_x/SiN_x stacks on 5 Ω·cm n-type Cz-Si wafers; (IV) the B-doped p^{++} sample with a symmetric double-sided laser doping the B-doped p^+ sample and passivation with AlO_x/SiN_x stacks on 5 Ω·cm n-type Cz-Si wafers; (V) the SiO_x/n^+-poly-Si sample with a symmetric double-sided SiO_x/n^+-poly-Si layer with AlO_x/SiN_x stacks on 5 Ω·cm n-type Cz-Si wafers; (VI) the SiO_x/p^+-poly-Si sample with a symmetric double-sided SiO_x/p^+-poly-Si layer and passivation with AlO_x/SiN_x stacks on 5 Ω·cm n-type Cz-Si wafers; (VII) the a-Si:H/nc-SiO_x:H(n^+) sample with a symmetric double-sided a-Si:H/nc-SiO_x:H(n^+) layer with indium-tin oxide (ITO) stacks on 5 Ω·cm n-type Cz-Si wafers; (VIII) the a-Si:H/nc-SiO_x:H(p^+) sample with a symmetric double-sided the a-Si:H/nc-SiO_x:H(p^+) layer with ITO stacks on 5 Ω·cm n-type Cz-Si wafers; (IX) the passivation sample with a symmetric double-sided passivation with AlO_x/SiN_x stack on 5 Ω·cm p-type Cz-Si wafers; the metallization-induced recombination ($J_{0e,\,metal}$) sample with metal contacts printed on one side of the (II), (IV), and (IX) with laser ablation samples on 5 Ω·cm p-type Cz-Si wafers and (V), (VI), (VII), and (VII)samples on 5 Ω·cm n-type Cz-Si wafers according to the previous methods [70]; the measurement of specific contact resistance (ρ_c) sample with H patterns on one side [70] of the (II), (IV), and (IX) with laser ablation sample on 0.5–2.1 Ω·cm n/p-type Cz-Si wafers and (V), (VI), (VII), and (VII) sample on 0.5–2.1 Ω·cm n-type Cz-Si wafers.

Then, we manufactured the three types of solar cells from commercially available 182×182 mm Cz–Si wafers with thickness of 140 ± 10 μm. Figure 2 shows the schematic depiction of the three types of structural cells. The fabrication sequence of PERC cell is shown in Table 1. p-Type Cz-doped Ga monocrystalline silicon wafers with the resistivity of 0.5–1.2 Ω·cm were textured in alkaline solution, followed by cleaning in HCl/HF mixed solution. The front P-selective emitters ($R_{\square,n++}$ = 135 Ω/sq, $R_{\square,n+}$ = 230 Ω/sq) were formed in a quartz tube furnace containing $POCl_3$ gas (Sevenstar) and laser doping technology with the width of 90–100 μm (DR laser, 532 nm, > 20 MKHz). After P diffusion, the rear side was polished by a mixed solution of KOH and polished additives. Subsequently, the front and rear passivation of the cells were achieved by thermal oxidation tube of SiO_x layer with thickness of 1–2 nm and PECVD of 80-nm-thick SiN_x dielectric stacks on the front side and ALD AlO_x 3–5 nm and PECVD 80-nm-thick SiN_x dielectric stacks on the rear side and then by laser ablation on the rear side with width of 20–35 μm (DR laser). The metallization was achieved by screen printing and firing of a metal paste using an H-patterned grid design on both sides of the wafers. A good contact is then formed using a firing temperature of 820°C.

The fabrication sequence of TOPCon cell is shown in Table 1. The n-type monocrystalline silicon wafers with a resistivity of 0.5–2.1 Ω·cm were also textured in alkaline solution and subsequently cleansed in an HCl/HF mixed solution. The front boron (B) SE ($R_{\square,p++}$ = 75 Ω/sq, $R_{\square,p+}$ = 230 Ω/sq) were formed in a quartz tube furnace containing BCl_3 gas (Sevenstar) and laser doping technology with the width of 90–100 μm (DR laser). After B diffusion, the rear side was also polished by a mixed solution of KOH and polished additives. The rear side stack,

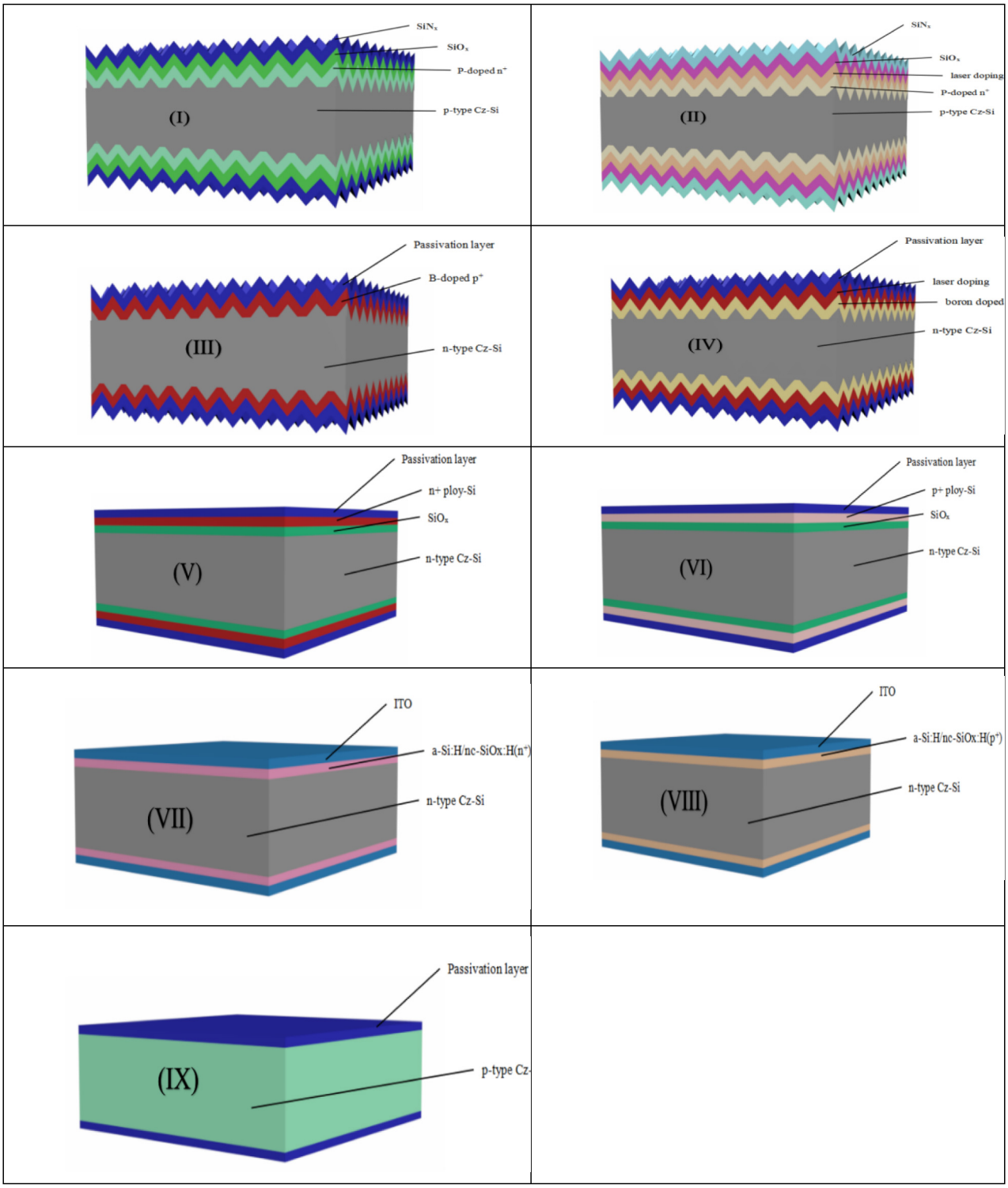

FIGURE 1 | Schematic illustration of the J_0 samples: (I) the P-doped n^+ sample with a symmetric double-sided P-diffused with SiO_x/SiN_x on 5 Ω·cm p-type Cz-Si wafers; (II) the P-doped n^{++} sample with a symmetric double-sided laser doping the P-doped n^+ sample with SiO_x/SiN_x on 5 Ω·cm p-type Cz-Si wafers; (III) the B-doped p^+ sample with a symmetric double-sided B-diffused and passivation with AlO_x/SiN_x stacks on 5 Ω·cm n-type Cz-Si wafers; (IV) the B-doped p^{++} sample with a symmetric double-sided laser doping the B-doped p^+ sample and passivation with AlO_x/SiN_x stacks on 5 Ω·cm n-type Cz-Si wafers; (V) the SiO_x/n^+-poly-Si sample with a symmetric double-sided SiO_x/n^+-poly-Si layer with AlO_x/SiN_x stacks on 5 Ω·cm n-type Cz-Si wafers; (VI) the SiO_x/p^+-poly-Si sample with a symmetric double-sided SiO_x/p^+-poly-Si layer and passivation with AlO_x/SiN_x stacks on 5 Ω·cm n-type Cz-Si wafers; (VII) the a-Si:H/nc-SiO_x:H(n^+) sample with a symmetric double-sided a-Si:H/nc-SiO_x:H(n^+) layer with ITO stacks on 5 Ω·cm n-type Cz-Si wafers; (VII) the a-Si:H/nc-SiO_x:H(p^+) sample with a symmetric double-sided the a-Si:H/nc-SiO_x:H(p^+) layer with ITO stacks on 5 Ω·cm n-type Cz-Si wafers; (IX) the passivation sample with a symmetric double-sided passivation with AlO_x/SiN_x stack on 5 Ω·cm p-type Cz-Si wafers.

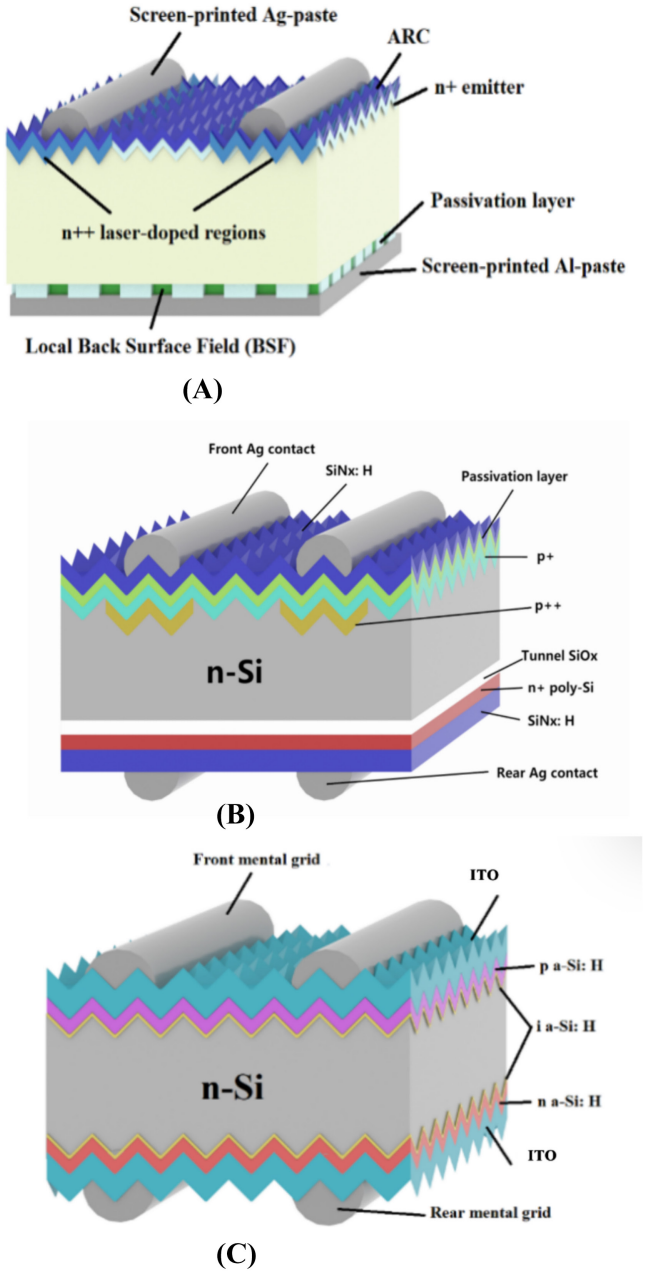

FIGURE 2 | Schematic depiction of cell structure for PERC (A), TOPCon (B), and SHJ (C) structure cells.

which consists of a SiO_x (1.4 ± 0.2 nm) layer and an intrinsic a-Si (100 ± 20 nm) layer, was formed by low-pressure chemical vapor deposition (LPCVD) and then annealed in a tube furnace at 880°C for 45 min using a mixture gas of $POCl_3$, O_2, and N_2 to form n^+-poly-Si layer. After removing BSG/PSG [71], the front and rear passivation of the cells were achieved by 3–5-nm-thick AlO_x by ALD and 80-nm-thick SiN_x dielectric stacks by PECVD. The metallization was achieved by screen printing and firing of a metal paste using an H-patterned grid design on both sides of the wafers (735 ± 5°C).

The fabrication sequence of SHJ cell also is shown in Table 1. The n-type monocrystalline silicon wafers with a resistivity of 1–3 Ω·cm were begun with an ozone cleaning process. The wafer gettering process was applied to improve its lifetime. Subsequently, the wafers were textured and cleaned by RCA solution. The intrinsic a-Si:H layers were deposited on both sides of wafers using a commercial PECVD system (13.56 MHz) at a low temperature. Then, the n-doped and p-doped nanocrystalline layers were deposited on the front and rear surfaces of the silicon substrate via a high-frequency PECVD system. Both the front and rear sides were deposited by indium tin oxide (ITO) films with the thicknesses of 100 and 120 nm, respectively. The metallization was achieved by screen printing and firing of a metal paste using an H-patterned grid design on both sides of the wafers (200°C, 30 min).

2.2 | Characterization

The current–voltage (I–V) parameters were measured using a vision tester. The implied V_{oc} (iV_{oc}) values of the controlled samples were determined by a lifetime tester under 1-sun illumination (WCT-120 Sinton, Boulder, CO, USA). The J_0 and $J_{0,metal}$ values of the samples were measured by WCT-120 Sinton and extracted at the excess carrier density of $3\times10^{15}\,cm^{-3}$ [60] (Boulder, CO, USA). The ρ_c of the screen-printed metallized contact with different samples was determined by the transfer length method (TLM) (GP-4 test). The optical reflectance of the cell was measured by PVE300-IVT. During these tests, the optical losses were analyzed by Current Loss Analysis Calculator V1.4 (the Solar Energy Research Institute of Singapore) [72].

3 | Results

3.1 | The Emitter Dark Saturation Current Density

To better investigate the effect of passivation, the J_0 values of different passivated contact layers were tested and characterized as shown in Figure 3. Both a-Si:H/nc-SiO_x:H(n^+) and a-Si:H/nc-SiO_x:H(p^+) layers with the thicknesses of a-Si:H 4–6 nm and nc-SiO_x:H 5–10 nm have the lowest J_0 values of about 2 fA/cm^2, shown in Figure 3A. It can explain why SHJ cell has a high V_{oc}, whereas the P-doped n^{++} and n^+ layers with the sheet resistances of 135 and 230 Ω/sq correspondingly have the highest J_0 values of about 18 and 60 fA/cm^2, respectively, which is consistent with the lowest V_{oc} of PERC solar cell. However, owing to AlO_x/SiN_x passivation, the B-doped p^{++} and p^+ layers ($R_{\square,p++}=75\,\Omega$/sq, $R_{\square,p+}=230\,\Omega$/sq) correspondingly have the lower J_0 values of about 8 and 25 fA/cm^2, respectively, than P doping layers. The J_0 values of the SiO_x/n^+-poly-Si layers with the thickness of 100 nm and the SiO_x/n^+-poly-Si layers with the thickness of 300 nm were about 4 and 6 fA/cm^2, respectively, which is higher than that of a-Si:H/nc-SiO_x:H. From the above analysis, it can be concluded that the a-Si:H/nc-SiO_x:H layer has the best passivation performance.

The metallization-induced recombination $J_{0,\,etal}$ for different layers is shown in Figure 3B. The $J_{0,metal}$ values of the P-doped n^{++} layer, SiO_x/n^+-poly-Si layer, and a-Si:H/nc-SiO_x:H(n^+) layer were about 500, 75, and 0 fA/cm^2, respectively, whereas the $J_{0,metal}$ values of p^+ layer on the Al-BSF, B-doped p^{++} layer, SiO_x/p^+-poly-Si layer, and a-Si:H/nc-SiO_x:H(p^+) layer were about 400, 250, 75, and 0 fA/cm^2, respectively. These values depend on the corrosiveness of the paste and sintering temperature. Owing to ITO layer, it can provide good

TABLE 1 | Preparation process of the three types of solar cell.

	Process flowchart		
Structure	**PERC**	**TOPCon**	**SHJ**
1	P-type Cz wafer	N-type Cz wafer	N-type Cz wafer
2	Alkaline texturization	Alkaline texturization	Alkaline texturization
3	Front P-doped n^+ emitter	Front B-doped p^+ emitter	Gettering
4	Laser doping n^{++}emitter	Laser doping p^{++}emitter	Front a-Si:H/nc-SiO_x:H(n^+) and rear a-Si:H/nc-SiO_x:H(p^+)
5	Wet chemical edge isolation	Formed SiO_x layer to protect n^{++} layer	ITO on the both sides
6	Front SiO_x passivation	Wet chemical edge isolation	Screen printing Ag paste on the both sides
7	Rear AlO_x/SiN_x passivation	SiO_x + i-Poly	—
8	Laser ablation the rear side	n^+-doped poly-Si	—
9	Screen printing Ag paste on the front side and Al paste on the rear side	AlO_x/SiN_x passivation	—
10	—	Screen printing AgAl paste on the front side and Ag paste on the rear side	—

conductivity, and then the corrosion of the paste on the a-Si:H/nc-SiO_x:H(n^+/p^+) layers can be ignored. Therefore, the $J_{0,metal}$ value is zero, which is consistent with the highest V_{oc} of SHJ solar cell. Meantime, the SiO_x/n^+-poly-Si layer also can provide a good conductivity, and then the intensity of paste erosion on its layer can be controlled. From the above analysis, we should balance the good conductivity and low corrosiveness of the paste on the metal area as one of the challenging and critical tasks in the PV market.

3.2 | The Specific Contact Resistance (ρ_c)

The plot of ρ_c values for different layers is shown in Figure 4. The n^+ layers, such as P-doped n^{++} emitter and SiO_x/n^+-poly-Si layer, have low ρ_c values with less than 1 mΩ·cm^2 owing to high solid solubility P in Si. However, a-Si:H/nc-SiO_x:H(n^+) layer is covered by the low parasitic absorption of ITO, resulting in low conductivity, and the high ρ_c is about 3 mΩ·cm^2. The B-doped p^{++} layer with deep junction depth of over 0.6 μm has a low ρ_c value of about 0.7 mΩ·cm^2, owing to deep corrosion of the Ag/Al paste [73]. And the a-Si:H/nc-SiO_x:H(p^+) layer has the lowest ρ_c of 0.3 mΩ·cm^2, which is attributed to ITO with high carrier concentration. However, p^+ layers, such as Al-BSF and SiO_x/p^+-poly-Si layer, have a high ρ_c value of about 3 mΩ·cm^2, owing to low doping concentration of these layers.

3.3 | Simulation

The PERC structure with the front side of selective P emitter and the rear side of AlO_x/SiN_x layer, TOPCon structure with the front side of selective B emitter and the rear side of SiO_x/n^+-poly-Si layer, and SHJ structure with the front side of a-Si:H/nc-SiO_x:H(n^+) layer and the rear side of a-Si:H/nc-SiO_x:H(p^+) layer were simulated (V_{oc}, *FF*) using Griddler 2.5, and the total saturation current density in the cell ($J_{o,total}$), the J_o on the front non-metallized area ($J_{0,front}$), and the rear non-metallized area ($J_{0,rear}$) were calculated using the measured values of J_o and $J_{o,metal}$ according to Equations (1)–(3), respectively. The saturation current density of the bulk material ($J_{o,bulk}$) was estimated to be 5 fA/cm^2 for n-type wafer and 20 fA/cm^2 for p-type wafer. The V_{oc} and *FF* values of the cells were calculated from $J_{o,total}$ and ρ_c using an ideal one-diode model, and the results are shown in Table 2. The SHJ solar cell had the highest V_{oc} of approximately 749 mV, thus obtaining a gain of over 20 and 50 mV compared to TOPCon and PERC cells, respectively, mainly owing to the $J_{o,total}$ reduction of 10 and 50 fA/cm^2, respectively. The TOPCon cell had a low ρ_c, resulting in a high *FF* of about 82.2%, followed by SHJ 81.5% without considering the contribution of V_{oc} to *FF*. Although the n^{++} layer on PERC cell had a low ρ_c, we could not obtain a high *FF*, mainly because of the high ρ_c of the p^+ layer.

$$\begin{aligned} J_{0,total} = \{&[(J_{0,metal}\times f)+(J_{0,p+}\times(1-f_{heavy,p++})\\ &+(J_{0,p++}\times(f_{heavy,p++}-f_{p++})](p-layer)\\ &+[J_{0,metal}\times f_{n++})+(J_{0,n+}\times(1-f_{heavy,n++})\\ &+(J_{0,n++}\times(f_{heavy,n++}-f)](n-layer)+J_{0,bulk}\} \end{aligned} \quad (1)$$

$$J_{0,p-layer} = (1-f_{p++})\times J_{0,p+}+((f_{heavy\ p++}-f\times J_{0,p++}) \quad (2)$$

$$J_{0,n-layer} = (1-f_{n++})\times J_{0,p+}+((f_{heavy\ n++}-f\times J_{0,n++}) \quad (3)$$

The J_0 loss was used to be discussed in order to understand the effects of passivation performance on the three types of solar cells. The results are shown in Figure 5. Compared to PERC

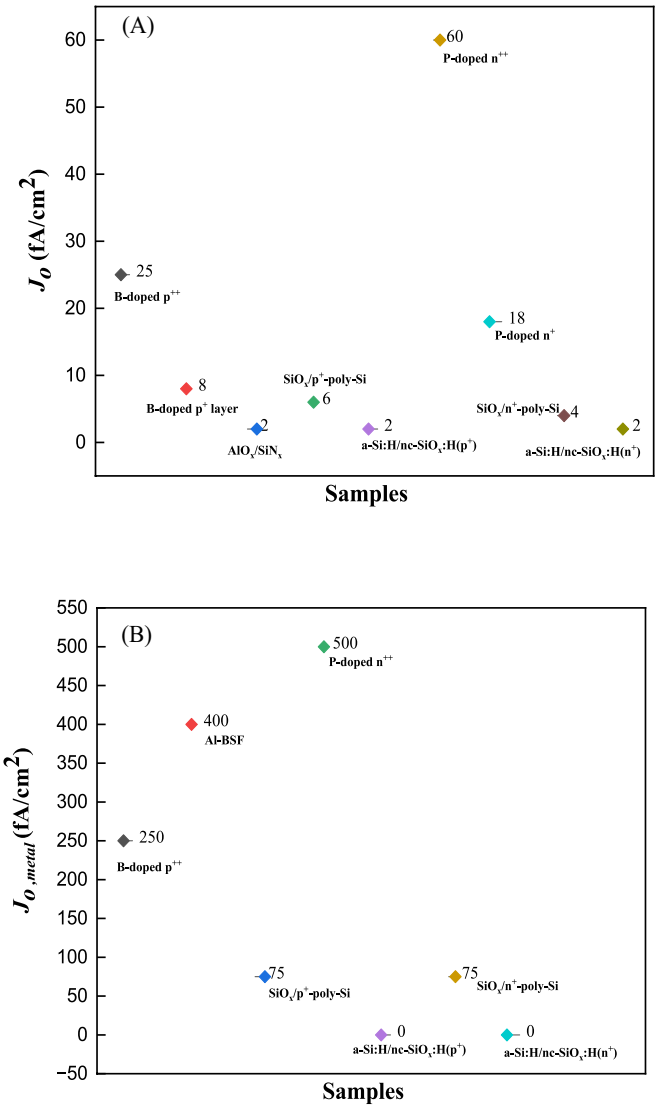

FIGURE 3 | (A) Emitter dark saturation current densities in the passivated regions of P-doped n^+/n^{++}, B-doped p^+/p^{++}, $SiO_x/n^+/p^+$-poly-Si, a-Si:H/nc-SiO_x:H(n^+/p^+) and the passivation sample, and (B) the metallization-induced recombination with metal contacts printed on one side of the P-doped n^{++}, B-doped p^{++}, $SiO_x/n^+/p^+$-poly-Si, a-Si:H/nc-SiO_x:H(n^+/p^+), and the passivation layer with laser ablation samples.

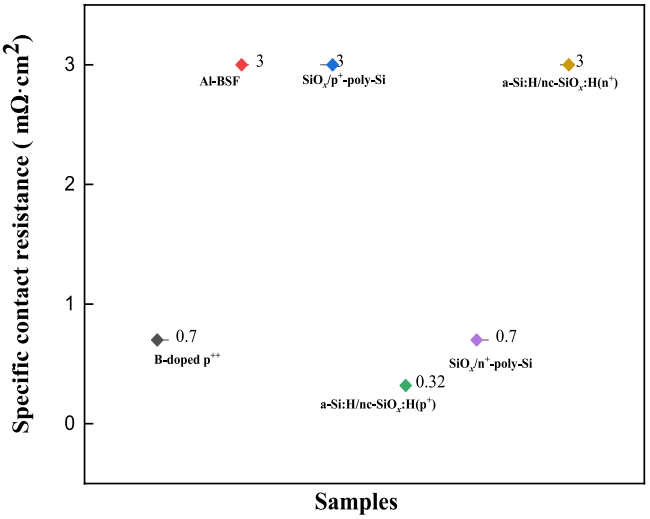

FIGURE 4 | Specific contact resistance for the P-doped n^{++}, B-doped p^{++}, $SiO_x/n^+/p^+$-poly-Si, a-Si:H/nc-SiO_x:H(n^+/p^+), and the passivation layer with laser ablation samples with H patterns on one side.

cell, the J_0 losses of TOPCon and SHJ cells have been reduced by 64% and 87%, respectively, which is mainly attributed to using the passivation contact layer such as SiO_x/n^+-poly-Si, a-Si:H/nc-SiO_x:H(n^+), and a-Si:H/nc-SiO_x:H(p^+) layers. At present, the main task of TOPCon solar cell is how to reduce the J_0 loss of p^+ layer, and the possible direction is aimed for the SiO_x/p^+-poly-Si layer to replace B-doped layer as the emitter. However, SHJ solar cell has almost perfect surface passivation performance.

3.4 | Cell Performance

The results of the iV_{oc} values and the effective carrier lifetime of the precursor structure at the excess carrier density of $1 \times 10^{15}\,cm^{-3}$ under 1-sun illumination are shown in Figure 6. The PERC solar cells did not show a good passivation performance, which exhibited a significantly low iV_{oc} value of about 716 mV. However, the SHJ solar cell exhibited the best passivation performance, a high iV_{oc} value of about 750 mV.

TABLE 2 | Detailed calculation of V_{oc} and *FF* using an ideal one-diode model from the measured values of J_o, $J_{o,metal}$, and ρ_c.

Bifacial solar cell			
Structure	**PERC (n^+pp^+)**	**TOPCon (p^+nn^+)**	**SHJ (n^+np^+)**
n^{++} layer (Ω/sq)	135	40	64
n^+ layer (Ω/sq)	220	40	64
$J_{0,n++}$ [fA/cm^2]	60	0	0
$J_{0,n+}$ [fA/cm^2]	18	4	2
$J_{0e,metal}$ (n^{++} fingers) [fA/cm^2]	500	75	0
Busbar fraction ($f_{busbar,n+}$) [%]	2.7%	0.4%	0.4%
Heavy doping layer fraction (n^{++} fingers) ($f_{heavyn+}$) [%]	7.6%	0.0%	0.0%
Metallized fraction (n^{++} fingers) (f_{n++}) [%]	1.6%	2.4%	1.4%
$J_{0,n\text{-}layer}$ [fA/cm^2]	21.3	3.9	2.0
p^{++} layer (Ω/sq)	80	130	80
p^+ layer (Ω/sq)	80	230	80
$J_{0,p++}$ [fA/cm^2]	50	25	0
$J_{0,p+}$ [fA/cm^2]	2	8	2
$J_{0e,metal}$ (p^{++} fingers) [fA/cm^2]	400.0	200.0	0.0
Busbar fraction ($f_{busbar,n+}$) [%]	0.30%	0.30%	0.35%
Heavy doping layer fraction (p^{++} fingers) ($f_{heavy\ p++}$) [%]	11.6%	7.8%	0.0%
Metallized fraction (p^{++} fingers) (f_{p++}) [%]	3.0%	1.6%	1.9%
$J_{0,p\text{-}layer}$ [fA/cm^2]	6.2	9.4	2.0
$J_{o,bulk}$ [fA/cm^2]	20.0	5.0	5.0
$J_{0e,total}$ [fA/cm^2]	67.7	23.3	8.9
ρ_c (p^{++} layer) [mΩ.cm^2]	3	0.7	0.3
ρ_c (n^{++} layer) [mΩ·cm^2]	1	0.7	0.3
V_{oc} (calculated) [mV]	697.0	723.0	749.0
FF [%]	80.6	82.2	81.5

Abbreviations: J_o, emitter dark saturation current density; $J_{o,metal}$, the dark saturation current density at metal contact; V_{oc}, open-circuit voltage; ρ_c, the specific contact resistance.

The TOPCon cell also get great advance, achieving a good passivation performance with iV_{oc} value of about 737 mV. This trend is strong for the effective carrier lifetime at the excess carrier density of 1×10^{15} cm^{-3}, and the order of median effective lifetime is the precursor structure of SHJ (2797 μs), TOPCon (1265 μs), and PERC cell (225 μs).

The *I–V* parameters of PERC, TOPCon, and SHJ cells are shown in Table 3. SHJ has a high V_{oc} of 748 mV, which is the same as the p*recursor* iV_{oc} and the simulated values, which indicated that the metallization-induced recombination can be ignored. Followed by V_{oc} 728 mV of TOPCon cell, it is indicated that the metallization-induced recombination caused a decrease in V_{oc} of up to 8 mV, especially in the p^+ region. But its V_{oc} value was higher than the simulated one, perhaps owing to un-considering the improvement bulk lifetime of wafer through the high-temperature process [55]. The PERC cell has the lowest V_{oc} value of 696 mV, which has a high decrease in V_{oc} of up to 20 mV owing to the metallization-induced recombination, which caused the direct contact between the silicon substrate and the metal paste. The order of J_{sc} value is TOPCon > PERC > SHJ, it is attributed to the parasitic absorption and surface passivation of the film layer. And the order of *FF* value is SHJ > TOPCon>PERC, which is attributed to the contact resistance and lateral resistance. From the above analysis, the efficiency performance of the cell is in the order of TOPCon > SHJ > PERC.

An analysis of the three types of solar cells using Suns–V_{oc} measurements is shown in Table 4. The SHJ solar cell has a high *pEff* of 26.2% owing to its high V_{oc} and *pFF*, followed by 26% of TOPCon and finally 23.9% of PERC without considering the loss of series resistance. This is consistent with the trend of *I–V* parameters. Mainly due to a high V_{oc} of 748 mV in SHJ, it is attributed to a decrease of 8 fA/cm^2 in J_{01} compared with TOPCon and a decrease of 56 fA/cm^2 in J_{01} compared with PERC. And there is a high *pFF* of 87.7%, indicating that low-temperature screen printing process cannot achieve good conductivity, which will be one of the challenging and critical tasks in SHJ cell. The PERC solar cell also has a high improvement in *pFF* increasing by 2%, indicating that there is a high damage on the passivation layer in high-temperature screen printing process.

3.5 | Failure Analysis

A current loss was used to be discussed in order to understand the effects of the three types of solar cells. The simulated optical reflectance was in agreement with the results of the experimental reflection without any adjustments (Figure 7A). In order to maintain the passivation performance of the surface, the SHJ solar cell has a large textured structure with high optical reflectance. However, considering the high corrosiveness of boron-doped silicon, the textured surface is controlled according to the low optical reflectance of small textured surface. The primary difference of an internal quantum efficiency (IQE) for PERC and SHJ/TOPCon solar cells occurred in the long-wavelength region of 600–1000 nm, which is mainly attributed to the bulk lifetime between p-type and n-type silicon wafers. The IQE for SHJ cell exhibited a poor response at

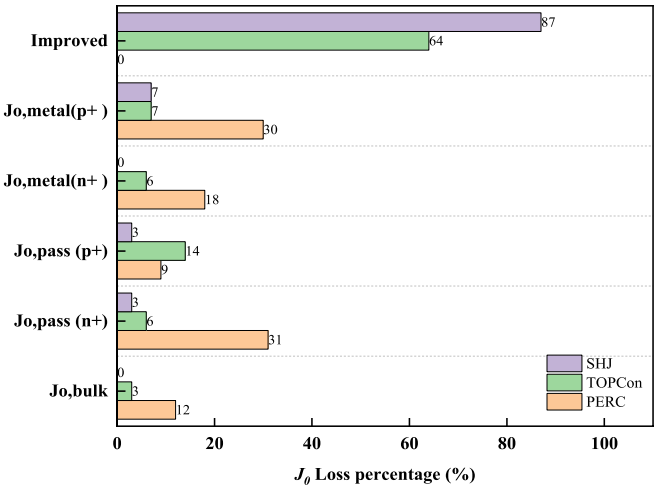

FIGURE 5 | The J_0 loss percentage for PERC, TOPCon, and SHJ cells.

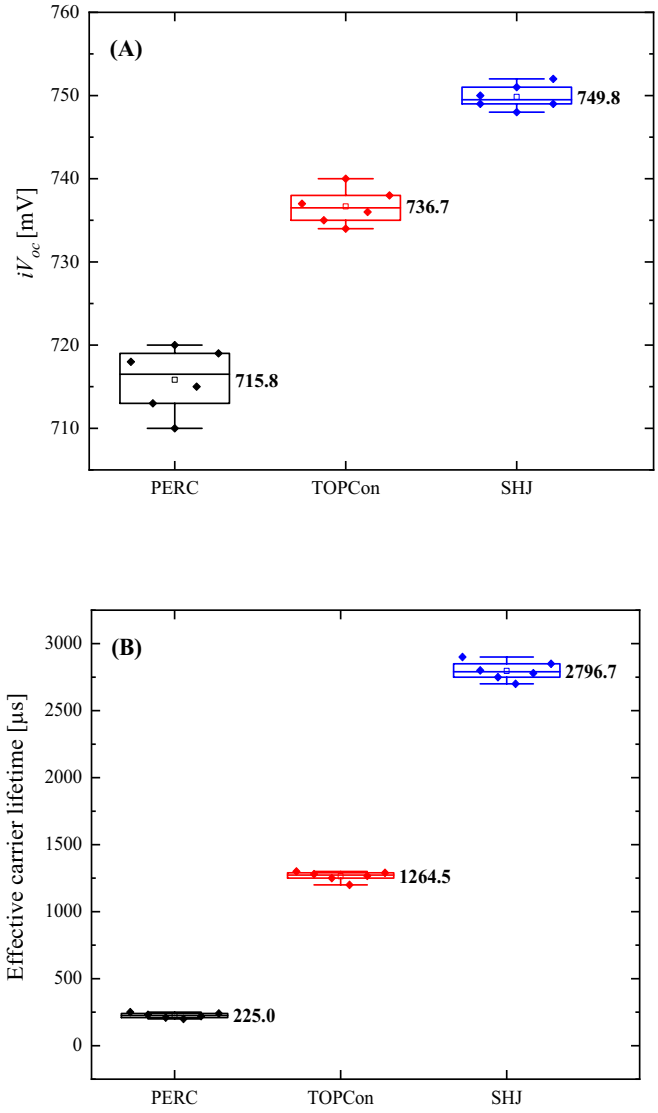

FIGURE 6 | iV_{oc} (A) and effective carrier lifetime (B) of PERC, TOPCon, and SHJ structure cells.

the wavelength of < 600 nm, owing to the optical reflectance and the parasitic absorption of a-Si:H/nc-SiO_x:H(n^+) layer. Meantime, the IQE for SHJ and TOPCon cells also exhibited a poor response at the wavelength of < 1000 nm, which is attributed to the parasitic absorption of a-Si:H/nc-SiO_x:H(p^+) and SiO_x/n^+-poly-Si layer.

TABLE 3 | *I–V* parameters of PERC, TOPCon, and SHJ cell.

Cell type	V_{oc} (mV)	J_{sc} (mA/cm^2)	*FF* (%)	E_{ff} (%)	Cell area (cm^2)
PERC	0.696	41.16	82.37	23.59	333.05
TOPCon	0.728	41.59	85.45	25.87	
SHJ	0.748	39.99	85.83	25.67	

TABLE 4 | *Suns–*V_{oc} parameters of PERC, TOPCon, and SHJ cells.

Cell type	V_{oc} (mV)	*pFF* (%)	*pEfficiency* (%)	J_{01} (fA/cm^2)
PERC	0.696	83.5	23.9	70
TOPCon	0.728	86	26	22
SHJ	0.748	87.7	26.2	14

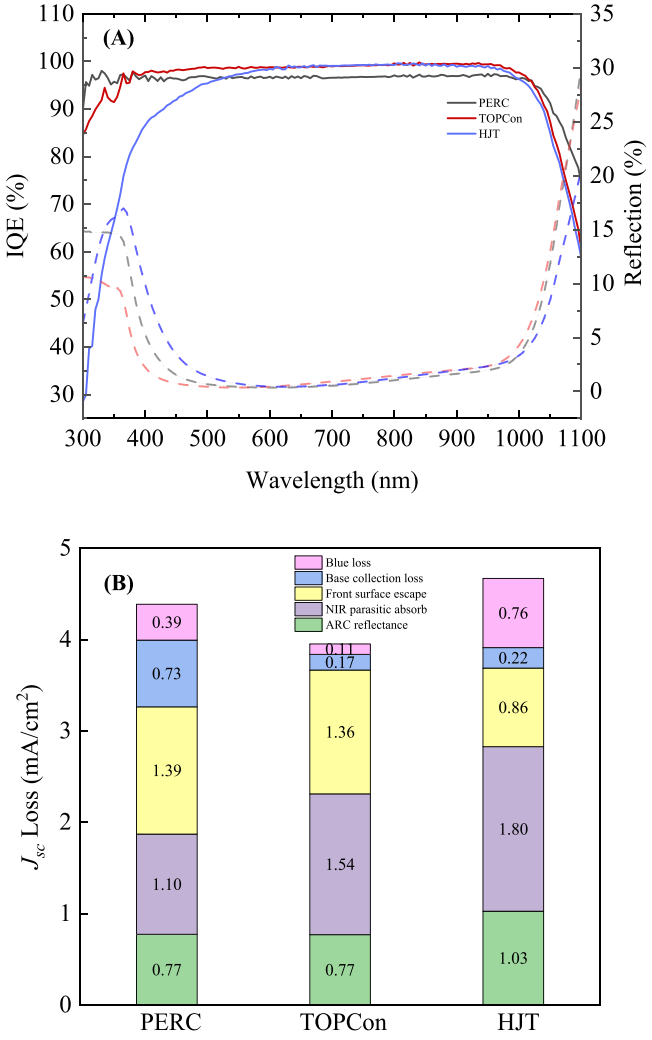

FIGURE 7 | IQE and reflection (A) and current loss analysis (B) of PERC, TOPCon, and SHJ cells.

The current loss analysis was carried out using the Current Loss Analysis Calculator V1.4 software (based on the Yablonovitch limit of 46.43 mA/cm^2) as shown in Figure 7B. Here, there are three primary advantages of TOPCon from SHJ solar cell: The one is "blue loss," in which the J_{sc} is increased by 0.65 mA/cm^2, which is related to the parasitic absorption of a-Si:H/nc-SiO$_x$:H(n$^+$) layer. The others are "ARC reflectance loss" and "NIR parasitic absorption loss," which can be benefit from low optical reflectance and the low parasitic absorption of SiO$_x$/n$^+$-poly-Si layer compared to a-Si:H/nc-SiO$_x$:H(p$^+$) layer. Although the "front surface escape loss" of TOPCon solar cell is worse than SHJ cell, it is indicated that the surface passivation of the boron doping layer is inferior to that of a-Si:H/nc-SiO$_x$:H(n$^+$) layer, it is consistent with the result of J_0. The PERC solar cell also has three primary advantages compared to SHJ solar cell: "blue loss," "ARC reflectance loss," and "NIR parasitic absorption loss." Compared to SHJ/TOPCon solar cell, the chief disadvantage of PERC solar cell is "base collection loss," which is mainly attributed to the bulk lifetime of p-type silicon wafer. From the above analysis, it can be concluded that TOPCon solar cell has a good optical performance. And reducing the optical loss is crucial for improving the efficiency of SHJ cell.

4 | Discussion

We have discussed the differences in optics, contact, and passivation performance among the three types of solar cells. We can now compare the carrier selectivity (S_{10}), according to the calculation, which assumes the non-contacted area with perfectly passivated (i.e., $J_0 = 0$) on the hole-selective contacts and electron-selective contacts. S_{10} values were calculated using the measured values of J_o and ρ_c, listed in Tables 5 and 6 according to Schmidt et al. [31]. The resulting selectivities $S_{10,e}$ and $S_{10,h}$, the efficiency-maximizing contacting area fraction $f_{e,max}$ and $f_{h,max}$, and the maximum efficiency $\eta_{e,max}$ and $\eta_{h,max}$ are calculated using Equations (4)/(5), (6)/(7), and (8). Among them, the $\eta_{max(S10)}$ is assuming a 2 Ω·cm n-type c-Si wafer with thickness of 110 μm with Lambertian light trapping (J_{sc} = 43.6 mA/cm^2) and intrinsic bulk recombination with a single contact of selectivity S_{10} [74]. Because of low J_o and ρ_c values for the electron-selective layers, it cannot find any significant differences in the $\eta_{e,max}$, which is compatible with [31]. However, for the hole-selective layers, the $S_{10,h}$ of Al-BSF layer has the lowest value of ~13.3, and the corresponding $\eta_{e,max}$ value is about 27.77%. This corresponds to earlier findings that a p-type 21.2%-efficient PERC cell with local screen-printed BSF contacts with J_o = 550 fA/cm^2 and ρ_c = 5 mΩ·cm^2 has a high limiting efficiency of 27.6% [31].

$$S_{10,e} = \log_{10}\left(\frac{V_{th}}{J_{0,e}\rho_{c,e}}\right) \quad (4)$$

$$S_{10,h} = \log_{10}\left(\frac{V_{th}}{J_{0,h}\rho_{c,h}}\right) \quad (5)$$

$$f_{max} = \rho_c / \rho_{max}(S_{10}) \quad (6)$$

$$\rho_{max} = \left(0.6271^{-1.085} + \left(1.620 \times 10^6\, e^{-\frac{S_{10}}{0.8891}}\right)^{-1.085}\right)^{-\frac{1}{1.085}} \Omega.cm^2 \quad (7)$$

TABLE 5 | The $S_{10,e}$, $f_{e,max}$, and $\eta_{e,max}$ on electron-selective contacts.

Electron-selective	$J_{0,e}$ [fA/cm^2]	ρ_c [mΩ.cm^2]	$S_{10,e}$	$f_{e,max}$ [%]	$\eta_{e,max}$ [%]
P-diffused n^{++}	60	1	14.6	1.01	28.93
P-diffused n^{+}	18	1	15.2	1.81	29.07
SiO_x-n^{+}-poly-Si	4	0.7	16	3.14	29.16
a-Si:H/nc-SiO_x:H(n^{+})	1	0.32	16.9	4.18	29.2
n-Type Si [62]	25	22	13.7	100	26.8

TABLE 6 | The $S_{10,h}$, $f_{h,max}$, and $\eta_{h,max}$ on the hole-selective contacts.

Electron-selective	$J_{0,h}$ [fA/cm^2]	ρ_c [mΩ.cm^2]	$S_{10,h}$	$f_{h,max}$ [%]	$\eta_{h,max}$ [%]
Al-BSF	400	3	13.3	0.86	27.77
B-diffused p^{++}	25	0.7	15.2	1.28	29.07
SiO_x-p^{+}-poly-Si	6	3	15.2	5.42	29.07
a-Si:H/nc-SiO_x:H(p^{+})	1	3.2	15.9	13.45	29.16

$$\eta_{max} = \left(\left(2.425\, S_{10} - 4.240\right)^{-19.52} + (29.21)^{-19.52} \right)^{-\frac{1}{19.52}} \% \quad (8)$$

We now evaluate the efficiency potential of the six types of solar cells. From the data of electron-selective contacts and hole-selective contacts in Tables 5 and 6, we calculate the maximum selectivity $S_{10,e\&h,max}$ using Equation (9), as shown in Table 7.

$$S_{e\&h,max} = \frac{1}{\left(\frac{1}{\sqrt{S_e}} + \frac{1}{\sqrt{S_h}}\right)^2} \quad (9)$$

The current PERC solar cell with an efficiency of 23.59% features an Al-BSF hole-selective layer and a P-diffused n^{++} electron-selective layer. The corresponding combined selectivity is $S_{10,e\&h,max}$ = 13.23 and the limiting efficiency to 27.5%. It is attributed to the industrially feasible path of SiO_2/SiN_x stacked layers to further enhance the potential of the n^{+} front emitter and to further decrease the saturation current density by 65 fA/cm and the ρ_c by 1.5 mΩ·cm^2. These data are higher than that of [31], which stated that the S_{10} value of an n^{+} contact for PERC is 12, owing to its high $J_{0,e}$ value of 109 fA/cm^2 passivated by SiN_x and a high contact resistance ρ_c of 0.26 Ω·cm^2 containing resistance contributions from the lateral current flow in the emitter and from the c-Si/metal interface.

And the current TOPCon solar cell with an efficiency of 25.87% features a B-diffused p^{++} hole-selective layer and a SiO_x-n^{+}-poly-Si electron-selective layer. The corresponding combined selectivity is $S_{10,e\&h,max}$ = 14.87 and the limiting efficiency to 29.01%, owing to its low ρ_c value of 0.7 mΩ·cm^2 of the B-diffused p^{++} hole-selective layer, which is lower than that of TOPCon solar cell with SiO_x/poly-Si(p^{+}) by chemical oxide/PECVD as hole-selective layer with a high ρ_c of 8 mΩ·cm^2, resulting in $S_{10,e\&h,max}$ of 14.2 and the potential efficiency of 28.7% [31].

The current mass production solar cell with an efficiency of 25.67% features an a-Si:H/nc-SiO_x:H(p^{+}) hole-selective layer and an a-Si:H/nc-SiO_x:H(n^{+}) electron-selective layer. The corresponding combined selectivity is $S_{10,e\&h,max}$ = 15.67 and the limiting efficiency to 29.14%. However, the SHJ solar cell features an a-Si:H(i)/a-SiH(p) hole-selective layer and an a-Si:H(i)/a-SiH(n) electron-selective layer, which have a high ρ_c value of 0.4 and 0.1 Ω·cm^2, respectively [31]. This points to the reason why the a-Si:H(i)/a-Si:H contacts offer a lower $S_{10,e\&h,max}$ value of 13.2 and the lower efficiency potential of 27.5% than the a-Si:H/nc-SiO_x:H layers [31].

Though we calculated the optimum actual fraction of cells with the above n-type Si wafer and the hole contact, as well as the electron contact, the maximum efficiency $\eta_{b,e,h,max}$ of PERC, TOPCon, and SHJ solar cells were 26.8%, 27.98%, and 28.12%, respectively. The maximum efficiency with metal shading ($\eta_{b,e,h,m,max}$) were calculated by using Equation (10), as shown in Table 7.

$$\eta_{b,e,h,m,max} = \left(J_{sc} - \mathrm{A} \times f_{front}\right) / J_{sc} \times \eta_{b,e,h,m,max} \quad (10)$$

where J_{sc} is about 43.6 mA/cm^2, A denotes the current loss value ratio of approximately 0.44 mA/cm^2/% under 1% contacting area on the front surface of solar cell according to Griddler simulation calculations, and f_{front} represents the contacting area fraction on the front side of solar cell.

Using Equation (10), the $\eta_{b,e,h,m,max}$ of PERC solar cell had gone down to 26.42%. Similarly, the $\eta_{b,e,h,m,max}$ of TOPCon cell was 27.62%; however, the $\eta_{b,e,h,m,max}$ of SHJ cell decreased to 26.91% owing to the high front contacting area fraction. The next-generation product is back-contact (BC) structure without metal shading. This allows for good passivation on the front surface without contact constraints. Then, we design three types of BC structure cells, which can achieve mass production, including hybrid passivated back-contact (HPBC), TOPCon

TABLE 7 | Combined selectivity $S_{10,e\&h}$, contact area fraction $f_{e,max}$ of electron-selective layer, contact area fraction $f_{h,max}$ of hole-selective layer, and maximum efficiency $\eta_{e,h,max}$, $\eta_{e,max}$, and $\eta_{b,e,h,m,max}$, are listed for all contact combinations of Tables 5 and 6. These numbers are determined using Equations (4)–(9).

Structure	Hole layer	Electron layer	$S_{10,e\&h}$	$f_{e,max}$ [%]	$f_{h,max}$ [%]	$\eta_{e,h,max}$ [%]	$S_{10,b\&e\&h}$	$\eta_{b,e,h,max}$ [%]	$\eta_{b,e,h,m,max}$ [%]
PERC (n^+np^+)	Al-BSF	P-diffused n^{++}	13.16	1.39	0.93	27.5	12.77	26.8	26.42
TOPCon (p^+nn^+)	B-diffused p^{++}	SiO_x-n^+-poly-Si	14.87	3.24	1.29	29.01	13.48	27.98	27.62
SHJ (n^+np^+)	a-Si:H/nc-SiO_x:H(p^+)	a-Si:H/nc-SiO_x:H(n^+)	15.67	4.28	13.52	29.14	13.59	28.12	26.91
HPBC (nn^+p^+)	Al-BSF	SiO_x-n^+-poly-Si	13.29	4.23	0.88	27.71	12.86	26.96	26.96
TBC (nn^+p^+)	SiO_x-p^+-poly-Si	SiO_x-n^+-poly-Si	15.12	4.34	5.94	29.06	13.59	27.99	27.99
HBC (nn^+p^+)	a-Si:H/nc-SiO_x:H(p^+)	a-Si:H/nc-SiO_x:H(n^+)	15.67	4.28	13.52	29.14	13.59	28.12	28.12

FIGURE 8 | Schematic diagram of cell structure for (A) HPBC, (B) TBC, and (C) HBC solar cells.

back-contact (TBC), and HBC, as shown in Figure 8. The efficiency of $\eta_{b,e,h,m,max}$ was in the order of HBC (28.12%) > TBC (27.99%) > HPBC (26.96%). From the above analysis, we conclude that by exploiting its high potential with large-scale production, a close to perfect passivation of the non-contact area, the wide process window, and low cost are required. And it will be the next major challenge for transferring these new concepts to industrial solar cell production.

5 | Conclusions

We have studied the passivation performance, electrical performance, and optical performance of the solar cells with different passivated contact layers. The main conclusions were made as follows: The passivated contact layers including a-Si:H/nc-SiO_x:H(n^+), a-Si:H/nc-SiO_x:H(p^+), SiO_x/n^+-poly-Si, and SiO_x/n^+-poly-Si layers have the low $J_0 < 6\,fA/cm^2$, the low $J_{0,metal} < 100\,fA/cm^2$, and the low $\rho_c \leq 3\,m\Omega{\cdot}cm^2$, whereas the P-doped n^{++}, the B-doped p^{++}, and Al-BSF layer had a high $J_0 \geq 25\,fA/cm^2$ and

a high $J_{0,metal} \geq 250\,fA/cm^2$ despite having a low $\rho_c \leq 3\,m\Omega \cdot cm^2$, which limits the cell efficiency.

Then we designed the three types of solar cell (PERC, TOPCon, and SHJ), and their loss analysis was studied and compared. The SHJ cell has the highest passivation performance with a high V_{oc} of 748 mV due to a lowest J_{01} of about 14 fA/cm^2, but worst optical performance owing to the parasitic absorption of a-Si:H layer. A 728 mV of TOPCon cell was obtained owing to the low J_{01} of SiO_x-n^+-poly-Si layer and good optical performance. The PERC cell has the lowest V_{oc} of 696 mV, which has a high decrease in V_{oc} of up to 20 mV owing to the metallization-induced recombination, which caused the direct contact between the silicon substrate and the metal paste. From the above analysis, the disadvantage of PERC solar cell is "base collection loss." The increasing *FF* and J_{sc} values are the challenging and critical tasks in SHJ cell. And the p^+ layer recombination is one of the critical tasks in TOPCon cell.

Through the S_{10} simulation, the PERC solar cell limits the efficiency to 26.42%, TOPCon 27.62%, and SHJ 26.91%. In the next-generation product BC structure, the order efficiency $\eta_{b,e,h,m,max}$ was followed in the order of HBC (28.12%) > TBC (27.99%) > HPBC (26.96%). From the perspective of limiting efficiency, TOPCon structure with high compatibility is suitable for bifacial BC solar cells, whereas SHJ structure with the parasitic absorption of a-Si:H layer and high contact resistivity is only suitable for BC solar cell. In conclusion, by exploiting its high potential with large-scale production, a close to perfect passivation of the non-contact area, the wide process window, and low cost are required. And transferring these new concepts to industrial solar cell production will be the next major challenge.

Author Contributions

Qinqin Wang: data curation, formal analysis, investigation, methodology, resources, software, writing – original draft, writing – review and editing, supervision. **Kaiyuan Guo:** data curation, formal analysis, investigation. **SiWen Gu:** formal analysis, methodology, review and editing. **Wei Huang:** data curation, methodology. **Hui Peng:** data curation, formal analysis, investigation. **Wangping Wu:** review and editing, supervision. **Jianning Ding:** review and editing, resources, supervision.

Acknowledgments

This work has been partially supported by the National Key Research and Development Program of China (2023YFB4202600, 2023YFB4202605) and the National Natural Science Foundation Youth Project (62304199).

Conflicts of Interest

The authors declare no conflicts of interest.

Data Availability Statement

The data that support the findings of this study are available from the corresponding author upon reasonable request.

References

1. H. Ullah, S. Czapp, S. Szultka, et al., "Crystalline Silicon (c-Si)-Based Tunnel Oxide Passivated Contact (TOPCon) Solar Cells: A Review," *Energies* 16 (2023): 715.

2. A. W. Blakers, A. Wang, A. M. Milne, J. H. Zhao, and M. A. Green, "22.8% Efficient Silicon Solar Cell," *Applied Physics Letters* 55 (1989): 1363–1365.

3. M. Fischer, M. Woodhouse, S. Herritsch, and J. Trube, "International Technology Roadmap for Photovoltaic (ITRPV)," (2023).

4. F. Fertig, R. Lantzsch, A. Mohr, et al., "Mass Production of p-Type Cz Silicon Solar Cells Approaching Average Stable Conversion Efficiencies of 22%," *Energy Procedia* 124 (2017): 338–345.

5. R. Chen, H. B. Tong, H. T. Zhu, et al., "23.83% Efficient Mono-PERC Incorporating Advanced Hydrogenation," *Progress in Photovoltaics: Research and Applications* 28 (2020): 1239–1247.

6. W. W. Deng, D. M. Chen, Z. Xiong, et al., "20.8% PERC Solar Cell on 156 mm × 156 mm P-Type Multicrystalline Silicon Substrate," in *44th IEEE Photovoltaic Specialists Conference* (2017), 2220–2226.

7. C. Vargas, G. Coletti, C. Chan, D. Payne, and Z. Hameiri, "On the Impact of Dark Annealing and Room Temperature Illumination on p-Type Multicrystalline Silicon Wafers," *Solar Energy Materials & Solar Cells* 189 (2019): 166–174.

8. U. Varshney, M. Abbott, A. Ciesla, et al., "Evaluating the Impact of SiN_x Thickness on Lifetime Degradation in Silicon," *IEEE Journal of Photovoltaics* 9 (2019): 601–607.

9. J. Schmidt, D. Bredemeier, and D. C. Walter, "On the Defect Physics Behind Light and Elevated Temperature-Induced Degradation (LeTID) of Multicrystalline Silicon Solar Cells," *IEEE Journal of Photovoltaics* 9 (2019): 1–7.

10. B. Hallam, M. Abbott, N. Nampalli, P. Hamer, and S. Wenham, "Influence of the Formation- and Passivation Rate of Boron-Oxygen Defects for Mitigating Carrier-Induced Degradation in Silicon Within a Hydrogen-Based Model," *Journal of Applied Physiology* 119 (2016): 065701.

11. C. Derricks, A. Herguth, G. Hahn, O. Romer, and T. Pernau, "Industrially Applicable Mitigation of BO-LID in Cz-Si PERC-Type Solar Cells Within a Coupled Fast Firing and Halogen Lamp Based Belt-Line Regenerator-A Parameter Study," *Solar Energy Materials & Solar Cells* 195 (2019): 358–366.

12. D. Stuwe, R. Keding, A. Salim, et al., "Inkjet-Printed Diffusion Sources," in *29th European Photovoltaic Solar Energy Conference and Exhibition* (2014), 976–979.

13. M. J. Kerr, J. Schmidt, A. Cuevas, and J. H. Bultman, "Surface Recombination Velocity of Phosphorus-Diffused Silicon Solar Cell Emitters Passivated With Plasma Enhanced Chemical Vapor Deposited Silicon Nitride and Thermal Silicon Oxide," *Journal of Applied Physics* 89 (2001): 3821–3826.

14. M. J. Kerr, J. Schmidt, and A. Cuevas. "Comparison of High Quality Surface Passivation Schemes for Phosphorus Diffused Emitters," in *16th European Photovoltaic Solar Energy Conference* (2000), 164–170.

15. R. S. Bonilla, B. Hoex, P. Hamer, and P. R. Wilshaw, "Dielectric Surface Passivation for Silicon Solar Cells: A Review," *Physica Status Solidi* 214 (2017): 1700293.

16. C. Leguijt, P. Loelgen, J. A. Eikelboom, et al., "Low-Temperature Surface Passivation of Silicon for Solar Cells," *Journal of the Electrochemical Society* 136 (1989): 518–523.

17. B. Hoex, J. J. H. Gielis, M. C. M. V. de Sanden, and W. M. M. Kessels, "On the c-Si Surface Passivation Mechanism by the Negative-Charge-Dielectric Al_2O_3," *Journal of Applied Physics* 104 (2008): 113703.

18. B. Hoex, J. Schmidt, P. Pohl, M. C. M. van de Sanden, and W. M. M. Kessels, "Silicon Surface Passivation by Atomic Layer Deposited Al_2O_3," *Journal of Applied Physics* 104 (2008): 044903.

19. G. Hahn, "Status of Selective Emitter Technology," in *25th European Photovoltaic Solar Energy Conference and Exhibition* (2010), 1091–1096.

20. M. H. Mohamed, A. Rohatgi, and T. Bobby, "A Review and Understanding of Screen-Printed Contacts and Selective-Emitter Formation," in *Proceedings of the 14th Workshop on Crystalline Silicon Solar Cells and Modules* (2004), 1–40.

21. H. Haverkamp, A. Dastgheib-Shirazi, B. Raabe, B. Felix, and H. Giso, "Minimizing the Electrical Losses on the Front Side: Development of a Selective Emitter Process From a Single Diffusion," in *23rd European Photovoltaic Solar Energy Conference and Exhibition* (2008), 2–4.

22. D. Rudolph, K. Peter, A. Meijer, O. Doll, and I. Köhler, "Etch Back Selective Emitter Process With Single $POCl_3$ Diffusion," in *26th European Photovoltaic Solar Energy Conference and Exhibition* (2011), 2–5.

23. P. Würfel and U. Würfel, *Physics of Solar Cells: From Basic Principles to Advanced Concepts* (Weinheim, Germany: Wiley, 2009).

24. J. Melskens, B. W. H. van de Loo, B. Macco, L. E. Black, S. Smit, and W. M. M. Kessels, "Passivating Contacts for Crystalline Silicon Solar Cells: From Concepts and Materials to Prospects," *IEEE Journal of Photovoltaics* 8 (2018): 373–388.

25. G. Beaucarne, G. Schubert, L. Tous, and J. Hoornstra, "Summary of the 7th Workshop on Metallization and Interconnection for Crystalline Silicon Solar Cells," in *7th Workshop on Metallization and Interconnection for Crystalline Silicon Solar Cells* (2017).

26. H. Hannebauer, T. Dullweber, T. Falcon, X. Chen, and R. Brendel, "Record Low Ag Paste Consumption of 67.7 mg With Dual Print," *Energy Procedia* 43 (2013): 66–71.

27. D. Erath, M. Pospischil, R. Keding, et al., "Comparison of Innovative Metallization Approaches for Silicon Heterojunction Solar Cells," *Energy Procedia* 124 (2017): 869–874.

28. F. Heinemeyer, C. Mader, D. Munster, T. Dullweber, and R. Brendel, "Inline High-Rate Thermal Evaporation of Aluminium for Novel Industrial Solar Cell Metallization," in *25th European Photovoltaic Solar Energy Conference and Exhibition* (2010), 2066–2068.

29. LONGi Solar 2019, "Single Crystal PERC cell Conversion Efficiency Breakthrough 24%! Longi Set Another World Record," enfsolar.com.

30. Y. Chen, D. Chen, P. P. Altermatt, et al., "Technology Evolution of the Photovoltaic Industry: Learning From History and Recent Progress," *Progress in Photovoltaics: Research and Applications* 31 (2023): 1194–1204.

31. R. Schmidt, R. Peibst, and R. Brendel, "Surface Passivation of Crystalline Silicon Solar Cells: Present and Future," *Solar Energy Materials and Solar Cells* 187 (2018): 39–54.

32. M. A. Green, "The Path to 25% Silicon Solar Cell Efficiency: History of Silicon Cell Evolution," *Progress in Photovoltaics: Research and Applications* 17, no. 3 (2009): 183–189.

33. M. A. Green, F. D. King, and J. Shewchun, "Minority Carrier MIS Tunnel Diodes and Their Application to Electron- and Photo-Voltaic Energy Conversion—I. Theory," *Solid-State Electronics* 17, no. 6 (1974): 551–561.

34. M. A. Green and A. W. Blakers, "Advantages of Metal-Insulator-Semiconductor Structures for Silicon Solar Cells," *Solar Cells* 8, no. 1 (1983): 3–16.

35. J. Y. Gan and R. M. Swanson, "Polysiliconemitters for Silicon Concentrator Solar cells," in *Proceedings 21st IEEE Photovoltaic Specialists Conference* (New York, IEEE, 1990), 245–250.

36. Y. H. Kwark and R. M. Swanson, "N-Type SIPOS and Poly-Si Emitters," *Solid-State Electronics* 30 (1987): 1121–1125.

37. F. Feldmann, M. Simon, M. Bivour, C. Reichel, M. Hermle, and S. W. Glunz, "Carrier-Selective Contacts for Si Solar Cells," *Applied Physics Letters* 104, no. 18 (2014): 181105.

38. K. K. Ng and H. C. Card, "Asymmetry in the SiO_2 Tunneling Barriers to Electrons and Holes," *Journal of Applied Physics* 51 (1980): 2153–2157.

39. S. P. Padi, M. Q. Khokhar, S. Chowdhury, E. C. Cho, and J. Yi, "Nanoscale SiOx Tunnel Oxide Deposition Techniques and Their Influence on Cell Parameters of TOPCon Solar Cells," *Transactions on Electrical and Electronic Materials* 22 (2021): 557–566.

40. "Up to 26.5%, TOPCon, HJT, BC Solar Cells Conversion Efficiency List!," Jibang New Energy Network, (n.d.), accessed June 11, 2024, https://www.energytrend.cn/news/20240410-135027.html.

41. Q. Q. Wang, K. Y. Guo, L. Yuan, et al., "Boron Tube Diffusion Process Parameters for High-Efficiency n-TOPCon Solar Cells With Selective Boron Emitters," *Solar Energy Materials & Solar Cells* 253 (2023): 112231.

42. Y. Tao, K. Madani, E. Cho, B. Rounsaville, V. Upadhyaya, and A. Rohatgi, "High-Efficiency Selective Boron Emitter Formed by Wet Chemical Etch-Back for n-Type Screen-Printed Si Solar Cells," *Applied Physics Letters* 110, no. 2 (2017): 021101.

43. T. Panda, S. Sadhukhan, S. Acharyya, et al., "Impact of Multi-busbar Front Grid Patterns on the Performance of Industrial Type c-Si Solar Cell," *Solar Energy* 236 (2022): 790–801.

44. H. Hannes, S. Felix, K. Eve, and G. Johannes, "Understanding Current Paths and Temperature Distributions During 'Laser Enhanced Contact Optimization' (LECO)," *AIP Conference Proceedings* 2826 (2023): 040002.

45. R. Mayberry, K. Myers, V. Chandrasekaran, A. Henning, H. Zhao, and U. E. Hofmüller, "Laser Enhanced Contact Optimization (LECO) and LECO-Specific Pastes–A Novel Technology for Improved Cell Efficiency," in *36th European Photovoltaic Solar Energy Conference and Exhibition* (2019).

46. E. Krassowski, S. Großer, M. Turek, and H. Höffler, "Laser Enhanced Contact Optimization–A Novel Technology for Metal-Semiconductor-Contact Optimization for Crystalline Silicon Solar Cells," in *37th European Photovoltaic Solar Energy Conference and Exhibition* (2020).

47. D. Ourinson, G. Emanuel, K. Rahmanpour, et al., "Laser-Powered Co-firing Process for Highly Efficient Si Solar Cells," *IEEE Journal of Photovoltaics* 11, no. 2 (2021): 282–288.

48. S. Dasgupta, Y. W. Ok, V. D. Upadhyaya, et al., "Novel Process for Screen-Printed Selective Area Front Polysilicon Contacts for TOPCon Cells Using Laser Oxidation," *IEEE Journal of Photovoltaics* 12, no. 6 (2022): 1282–1288.

49. S. Schäfer, A. Mercker, A. Köhler, et al., "Role of Oxygen in the UV-ps Laser Triggered Amorphization of Poly-Si for Si Solar Cells With Local Passivated Contacts," *Journal of Applied Physics* 129, no. 13 (2021): 133103.

50. Jinko Solarn, (n.d.), accessed March 17, 2023, https://www.jinkosolar.com/en/site/newsdetail/1827.

51. F. Haase, C. Hollemann, S. Schäfer, et al., "Laser Contact Openings for Local Poly-Si-Metal Contacts Enabling 26.1%-Efficient POLO-IBC Solar Cells," *Solar Energy Materials & Solar Cells* 186 (2018): 184–193.

52. M. K. Stodolny, M. Lenes, Y. Wu, et al., "N-Type Polysilicon Passivating Contact for Industrial Bifacial n-Type Solar Cells," *Solar Energy Materials & Solar Cells* 158 (2016): 24–28.

53. W. Fuhs, K. Niemann, and J. Stuke, "Heterojunctions of Amorphous Silicon and Silicon Single Crystals," *AIP Conference Proceedings* 20 (1974): 345.

54. M. Tanaka, M. Taguchi, T. Matsuyama, et al., "Development of New a-Si/c-Si Heterojunction Solar Cells: ACJ-HIT (Artificially Constructed Junction-Heterojunction With Intrinsic Thin-Layer)," *Japanese Journal of Applied Physics* 31, no. 11R (1992): 3518.

55. Y. Hamakawa, K. Fujimoto, K. Okuda, Y. Kashima, S. Nonomura, and H. Okamoto, "New Types of High Efficiency Solar Cells Based on a-Si," *Applied Physics Letters* 43 (1983): 644–646.

56. H. Matsuura, T. Okuno, H. Okushi, and K. Tanaka, "Electrical Properties of n-Amorphous/p-Crystalline Silicon Heterojunctions," *Journal of Applied Physics* 55 (1984): 1012–1019.

57. S. J. Bao, L. Y. Yang, J. Huang, et al., "The Rapidly Reversible Processes of Activation and Deactivation in Amorphous Silicon Heterojunction Solar Cell Under Extensive Light Soaking," *Journal of Materials Science: Materials in Electronics* 32 (2021): 4045–4052.

58. A. Descoeudres, J. Horzel, B. Paviet-Salomon, et al., "The Versatility of Passivating Carrier-Selective Silicon Thin Films for Diverse High-Efficiency Screen-Printed Heterojunction-Based Solar Cells," *Progress in Photovoltaics: Research and Applications* 28 (2019): 569–577.

59. K. Yamamoto, K. Yoshikawa, H. Uzu, and D. Adachi, "High-Efficiency Heterojunction Crystalline Si Solar Cells," *Japanese Journal of Applied Physics* 57 (2018): 08RB20.

60. C. Yu, M. Yang, G. Q. Dong, et al., "Development of Silicon Heterojunction Solar Cell Technology for Manufacturing," *Japanese Journal of Applied Physics* 57 (2018): 08RB15.

61. H. Lin, M. Yang, X. Ru, et al., "Silicon Heterojunction Solar Cells With up to 26.81% Efficiency Achieved by Electrically Optimized Nanocrystalline-Silicon Hole Contact Layers," *Nature Energy* 8 (2023): 789–799.

62. W. Shockley and H. J. Queisser, "Detailed Balance Limit of Efficiency of p-n Junction Solar Cells," *Journal of Applied Physics* 32 (1961): 510–519.

63. "LONGi Sets a New World Record of 27.09% for the Efficiency of Silicon Heterojunction Back-Contact (HBC) Solar Cells," https://www.longi.com/en/news/heterojunction-back-contact-battery.

64. "LONGi Unveils HBC Cell With Record 27.3% Conversion Efficiency," pv-tech.org.

65. L. Mazzarellaa, A. B. Morales-Vilchesa, L. Korteb, R. Schlatmanna, and B. Stannowskia, "Ultra-Thin Nanocrystalline n-Type Silicon Oxide Front Contact Layers for Rear Emitter Silicon Heterojunction Solar Cells," *Solar Energy Materials & Solar Cells* 179 (2018): 386–391.

66. P. Cuony, D. Alexander, I. Perez-Wurfl, et al., "Silicon Filaments in Silicon Oxide for Next-Generation Photovoltaics," *Advanced Materials* 24 (2012): 1182–1186.

67. M. Klingsporn, S. Kirner, C. Villringer, et al., "Resolving the Nanostructure of Plasma-Enhanced Chemical Vapor Deposited Nanocrystalline SiO_x Layers for Application in Solar Cells," *Journal of Applied Physics* 119 (2016): 223104.

68. S. Zih-Yu, H. Wen-Chi, Y. Hsiang-Wei, J. Chang, and C. Ming-Yu, "A Study of Improving Wafer Quality With the Phosphorus Gettering Process on Silicon Heterojunction Solar Cells," in *European Photovoltaic Solar Energy Conference and Exhibition* (2016), 940–942.

69. S. Takeshita, K. Nakayama, T. Isobe, T. Sawayama, and S. Niikura, "Optical Properties of Transparent Wavelength-Conversion Film Prepared From YVO[sub 4]:Bi[sup 3+],Eu[sup 3+] Nanophosphors," *Journal of the Electrochemical Society* 156, no. 9 (2009): J273–J277.

70. Q. Q. Wang, H. Peng, S. W. Gu, et al., "High-Efficiency n-TOPCon Bifacial Solar Cells With Selective Poly-Si Based Passivating Contacts," *Solar Energy Materials & Solar Cells* 259 (2023): 112458.

71. Q. Q. Wang, W. P. Wu, D. M. Chen, et al., "Study on the Cleaning Process of n+-Poly-Si Wraparound Removal of TOPCon Solar Cells," *Solar Energy* 211 (2020): 324–335.

72. J. Wong, S. Raj, J. W. Ho, J. Q. Wang, and J. J. Lin, "Voltage Loss Analysis for Bifacial Silicon Solar Cells: Case for Two-Dimensional Large-Area Modeling," *IEEE Journal of Photovoltaics* 6, no. 99 (2017): 1421–1426.

73. Q. Q. Wang, W. P. Wu, Y. P. Li, et al., "Impact of Boron Doping on Electrical Performance and Efficiency of n-TOPCon Solar Cell," *Solar Energy* 227 (2021): 273–291.

74. R. Brendel and R. Peibst, "Contact Selectivity and Efficiency in Crystalline Silicon Photovoltaics," *IEEE Journal of Photovoltaics* 6, no. 6 (2016): 1413–1420.